# Low-energy charge transfer in collisions of $He^{2+}$ with H in a Debye plasma

Y. Zhang,[1] C. H. Liu,[1] Y. Wu,[1] J. G. Wang,[1] Y. Z. Qu,[2] and J. Yan[1]
[1]*Institute of Applied Physics and Computational Mathematics, P. O. Box 8009, Beijing 100088, China*
[2]*College of Material Sciences and Optoelectronic Technology, P. O. Box 4588, Beijing 100049, China*
(Received 24 August 2010; published 22 November 2010)

Charge transfer in collisions of $\alpha$ particles with ground-state H embedded in a Debye plasma is studied in the low-energy region from $10^{-4}$ eV to 5 keV. The screened Coulomb interaction is described by the Debye-Hückel potential. The relevant molecular potentials and coupling matrix elements are obtained using a modified multireference single-and double-excitation configuration interaction package. Total and state-selective cross sections in the nonradiative charge-transfer collisions from 60 eV to 5 keV are calculated using the quantum-mechanical molecular-orbital close-coupling method. Both optical-potential and semiclassical methods have been used in the investigation of the radiative charge transfer from $10^{-4}$ to 1 eV and 1 to $10^2$ eV, respectively. The total cross sections for the no-screening case are in good agreement with the existing data. The effects of the screened Coulomb potential on the electron-capture cross sections are discussed.

DOI: 10.1103/PhysRevA.82.052706 PACS number(s): 34.70.+e, 34.20.−b

## I. INTRODUCTION

Heavy-particle collision processes (including charge transfer, excitation, ionization, etc.) in hot, dense plasmas have attracted much attention for many years [1–6] due to their crucial role in determining radiation and transport properties. Charge transfer in collisions of highly charged ions with neutral atoms and molecules is of particular interest because of the importance of electron-capture processes not only in basic atomic physics, astrophysics, and plasma physics, but also in various practical applications. Among the most prototypical, few-body atomic collision processes is the one-electron $(HeH)^{2+}$ collision system, in which an electron is captured from atomic hydrogen by an impacting $\alpha$ particle. In addition to the fundamental importance of understanding the process quantitatively, detailed investigation of $He^{2+}$ + H (D, T) is highly desired in fusion energy research. In a fusion reactor, fast helium ions $^4He^{2+}$ are produced in fusion plasmas by the reaction between deuterium (D) and tritium (T). As $\alpha$ particles are slowed down by elastic collision and reach the cool, dense edge region of the fusion device, they can recombine into an excited $He^+$ state in part by collision with hydrogen and contribute to radiative cooling [7].

Numerous theoretical [8–18], as well as experimental [19–22] studies of the process over a wide range of impact energies and final state quantum levels have been made during the last several decades. However, to the best of our knowledge, few investigations have considered the effects of plasma screening of the Coulomb interaction between the charged particles. These effects are related to the modified structure of composite particles and may profoundly change the dynamics of collision and radiative processes in the system. Recent studies exploring the collision dynamics of the $He^{2+}$ + H(1*s*) system embedded in a Debye plasma by Liu *et al.* [23] using the Debye-Hückel potential and the two-center atomic orbital close-coupling approach in the high-energy range from 5 to 300 keV/u have demonstrated that the screening of Coulomb interactions in the system not only progressively reduces the number of available excitation and electron-capture channels when the strength of the plasma screening increases, but also introduces changes in the values of direct and exchange couplings, thus affecting the magnitude and energy behavior of the cross sections.

In the present work, we explore the effects of Coulomb interaction screening on the electron-capture processes in low-energy collisions

$$He^{2+} + H(1s) \rightarrow He^+(2l) + H^+ \quad (1)$$

$$\rightarrow He^+(1s) + H^+ + h\nu \quad (2)$$

for center-of-mass collision energy $E_{\mathrm{c.m.}}$ below 5 keV where the quasimolecular collision is kept in its simplest form. In our calculation, the interactions between charged particles are described by the Debye-Hückel potential $V(r) = \pm\frac{Z_1 Z_2}{r} e^{-r/D}$, where $D = (k_B T_e/4\pi n_e)^{1/2}$ is the Debye screening length, $T_e$ and $n_e$ are the plasma electron temperature and density, and $k_B$ is the Boltzmann constant. The Debye-Hückel potential is valid only when the Coulomb coupling parameter $\Gamma = 1/(ak_B T_e)$ and plasma nonideality parameter $\gamma = 1/(Dk_B T_e)$ satisfy the conditions $\Gamma \leqslant 1$, $\gamma \ll 1$, where $a = [3/(4\pi n_e)]^{1/3}$ is the average interparticle distance [3,6]. There is a wide class of laboratory and astrophysical plasmas (Debye plasmas) in which these conditions hold. For example, inertial confinement fusion plasmas with $T_e \sim$ 1–10 keV and $n_e \sim (1\text{–}10)\times 10^{24}$ cm$^{-3}$ belong to this type of plasma.

The total and state-selective charge-transfer cross sections in process (1) are calculated by using the quantum-mechanical molecular orbital close-coupling (QMOCC) method. Two approaches, the adiabatic optical-potential method and the semiclassical JWKB method, are applied to calculate the capture cross section of the radiative charge-transfer in process (2). The outline of the paper is as follows. In Sec. II, a brief description of the theoretical methods is given; in Sec. III, we present the results and discussion as well as comparisons of the available theoretical and experimental data. Section IV briefly gives a summary of the work and the most important conclusions.

## II. THEORETICAL METHOD

### A. Electronic structure calculation and QMOCC method

In the present work, the adiabatic potential curves of the electronic states of the $(HeH)^{2+}$ system are calculated by

 

using the *ab initio* multireference single- and double-excitation configuration interaction method (MRD-CI package) [24]. Since a Gaussian basis is used in the code and one handy property of Gaussian functions is that the product of two Gaussians is still a Gaussian, we found it numerically convenient to represent the Debye-Hückel interaction between nuclei and electron as a superposition of Gaussians, $\frac{e^{-\alpha r}}{r} = \frac{1}{r}\sum_i c_i e^{-\alpha_i r^2}$, where $c_i$ and $\alpha_i$ are fitting parameters, and to appropriately modify the one-electron integral in the MRD-CI code. In our calculation, ten Gaussians were used in the above superposition, and the adequacy of the approximation of the exponent in the Debye-Hückel potential has been checked in Ref. [25]. A (21*s*,17*p*,5*d*) contracted to [19*s*,17*p*,5*d*] basis set is used to describe helium, and an (18*s*,14*p*) contracted to [14*s*,14*p*] basis set is employed for hydrogen. The basis is large enough to ensure adequate solutions for various screening lengths $D$ in the Debye-Hückel potential.

The QMOCC method has been described thoroughly in the literature (e.g., Kimura and Lane [26], Zygelman *et al.* [27], and Wang *et al.* [28]) and is only briefly discussed here. It involves solution of a coupled set of second-order differential equations using the log-derivative method of Johnson [29]. In the adiabatic representation, transitions between channels are driven by radial and rotational ($A^{\rm rad}$ and $A^{\rm rot}$) couplings of the vector potential $A(\vec{R})$, where $\vec{R}$ is the internuclear distance vector. Since the adiabatic description contains first- and second-order derivatives, it is numerically convenient to make a unitary transformation [27,30,31] to a diabatic representation

$$U(R) = W(R)\,[V(R) - P(R)]\,W^{-1}(R) \tag{3}$$

and

$$dW(R)/dR + W(R)A^{\rm rad}(R) = 0, \tag{4}$$

where $U(R)$ is the diabatic potential matrix, $V(R)$ is the diagonal adiabatic potential, $W(R)$ is a unitary transformation matrix, and $P(R)$ is the rotational matrix of the vector potential $A(\vec{R})$ [28,32,33]. With the diabatic potentials and couplings, the coupled set of second-order differential equations is solved to obtain the $K$ matrix from the scattering amplitude after a partial-wave decomposition (see, e.g., Zygelman *et al.* [27]). The electron-capture cross section is then given by

$$\sigma_{\alpha\to\beta} = \frac{\pi g_\alpha}{k_\alpha^2}\sum_J (2J+1)|(S_J)_{\alpha\beta}|^2, \tag{5}$$

where the $S$ matrix is defined as

$$\underline{S}_j = [\underline{I} + i\underline{K}_j]^{-1}[\underline{I} - i\underline{K}_j], \tag{6}$$

$\underline{I}$ is the identity matrix, $k_\alpha$ denotes the wave number for center-of-mass motion of the initial ion-atom channel, and $g_\alpha$ is an approach probability factor of the initial channel $\alpha$. Electron translation factors (ETF's) [26] have been included in the current calculations since we found it is quite important for collision energies around and above 1 keV in the $(HeH)^{2+}$ collision system. By applying the common ETF's [34], the radial and rotational coupling matrix elements between states $\psi_K$ and $\psi_L$ are transformed respectively into [35]

$$\begin{aligned}&\langle\psi_K|\partial/\partial R - (\varepsilon_K - \varepsilon_L)z^2/2R|\psi_L\rangle,\\ &\langle\psi_K|iL_y + (\varepsilon_K - \varepsilon_L)zx|\psi_L\rangle,\end{aligned} \tag{7}$$

where $\varepsilon_K$ and $\varepsilon_L$ are the electronic energies of states $\psi_K$ and $\psi_L$, and $z^2$ and $zx$ are the components of the quadrupole moment tensor. The method described above is carried out for each partial wave $J$ until the cross section converges.

### B. Optical-potential method and semiclassical method

The optical-potential method for treating radiative charge transfer is described in detail by Zygelman and Dalgarno [36]. During the ion-atom collisions, the transition probability per unit time for the radiative spontaneous-emission process, i.e., the Einstein coefficient, is represented by the imaginary part of a complex optical potential. The scattering wave $F_I(\vec{R})$, where $R$ is the internuclear distance and the subscript $I$ denotes the initial upper molecular state, is obtained by solving the Schrödinger equation

$$\left[-\frac{1}{2\mu}\nabla_{\vec{R}}^2 + V_I(R) - E\right]F_I(\vec{R}) = \frac{i}{2}A(R)F_I(\vec{R}). \tag{8}$$

Here $E$ is the collision energy in the entrance channel, $\mu$ is the reduced mass, and $A(R)$ is the transition probability for the radiative transition given by

$$A(R) = \frac{4}{3c^3}|\vec{D}(R)|^2|V_I(R) - V_F(R)|^3, \tag{9}$$

where $c$ is the speed of light, and $V_I(R)$ and $V_F(R)$ are the adiabatic potential energies of the upper and the lower states, respectively. $\vec{D}(R)$ is the transition dipole defined by

$$\vec{D}(R) = \langle\psi_I|\vec{r}|\psi_F\rangle \tag{10}$$

in terms of the initial and final electronic wave functions.

The cross section for collision-induced radiative decay can be written as

$$\sigma(E) = \frac{\pi}{k_I^2}\sum_J^\infty (2J+1)\,[1 - \exp(-4\eta_J)], \tag{11}$$

where $\eta_J$ is the imaginary part of the phase shift for the $J$th partial wave of the radial Schrödinger equation, which is given in the distorted-wave approximation by

$$\eta_J = \frac{\pi}{2}\int_0^\infty dR\left|f_J^I(k_I R)\right|^2 A(R), \tag{12}$$

where $k_I = \sqrt{2\mu\,[E - V_I(\infty)]}$, and $f_J^I(k_I R)$ is the regular solution of the homogeneous radial equation

$$\begin{aligned}&\left\{\frac{d^2}{dR^2} - \frac{J(J+1)}{R^2} - 2\mu[V_I(R) - V_I(\infty)] + k_I^2\right\}\\ &\quad\times f_J^I(k_I R) = 0\end{aligned} \tag{13}$$

and is normalized asymptotically according to

$$f_J^I(k_I R) = \sqrt{\frac{2\mu}{\pi k_I}}\sin\left(k_I R - \frac{J\pi}{2} + \delta_J^I\right). \tag{14}$$

In order to extend the calculation to higher energy, by replacing the summation in Eq. (11) and applying the JWKB

approximation, one obtains the expression for the semiclassical cross section,

$$\sigma(E) = 2\pi\sqrt{\frac{2\mu}{E}}\int pdp\int_{R_I^{\mathrm{CTP}}}^{\infty} dR\frac{A(R)}{\sqrt{1-V_I(R)/E-p^2/R^2}} \tag{15}$$

where $p$ is the impact parameter and $R_I^{\mathrm{CTP}}$ is the classical turning point in the incoming channel [36,37]. For large energies ($E \gg V_I$), the double integral is nearly energy independent, and therefore $\sigma(E)$ varies as $1/E^{\frac{1}{2}}$ [38,39].

## III. RESULTS AND DISCUSSION

### A. $He^{2+} + H(1s) \rightarrow He^{+}(2l) + H^{+}$ collisions

In the low-impact-energy region, it is commonly accepted that charge transfer in $He^{2+} + H(1s)$ collisions is dominated by couplings between the initial state $2p\sigma$ and the final states $2s\sigma$, $3d\sigma$, and $2p\pi$. The electronic energies $\epsilon_n(R)$ versus the internuclear distance $R$ of the most important molecular states in the $(HeH)^{2+}$ collision system are shown in Figs. 1(a)–1(d) for the unscreened case and Debye length $D = 10.0$, 5.0, 2.0, respectively. In the large-$R$ limit the $2p\sigma$ molecular orbital becomes the $H(1s)$ atomic orbital, and the $2s\sigma$,$3d\sigma$,$2p\pi$ states correlate with the $He^{+}(2s,2p_0,2p_{\pm1})$ states. In the no-screening case, $2p\sigma$, the $2s\sigma$, $3d\sigma$, and $2p\pi$ states are degenerate as $R \rightarrow \infty$. The degeneracy is removed in the case with a screened Coulombic potential and the splitting between the initial state $2p\sigma$ and the final states $2s\sigma$,$3d\sigma$,$2p\pi$ increases when the Debye length $D$ decreases, as shown in Figs. 1(b)–1(d). Another significant screening effect is that all the binding energies shift up as the screening becomes stronger. In the extreme case, when $D = 2.0$ [Fig. 1(d)], $3d\sigma$ and $2p\pi$ are no longer bound states (not shown in the figure); thus the $2s\sigma$ state becomes the only possible final channel for the charge-transfer process. Further decreasing $D$ will eventually remove all the possible channels and the collision process (1) is completely forbidden. We also note there is a strong avoided crossing between $2p\sigma$ and $2s\sigma$ at about $R = 0.35$ when $D = 2.0$, as shown in Fig. 1(d). The avoided crossing that appears is also due to the Coulombic screening effect since in the united-atom limit the $2s\sigma$ and $2p\sigma$ orbitals become the $2s$ and $2p$ atomic orbitals of $Li^{2+}$, and the orbital energy of $Li^{2+}(2s)$ is lower than that of $Li^{2+}(2p)$ when

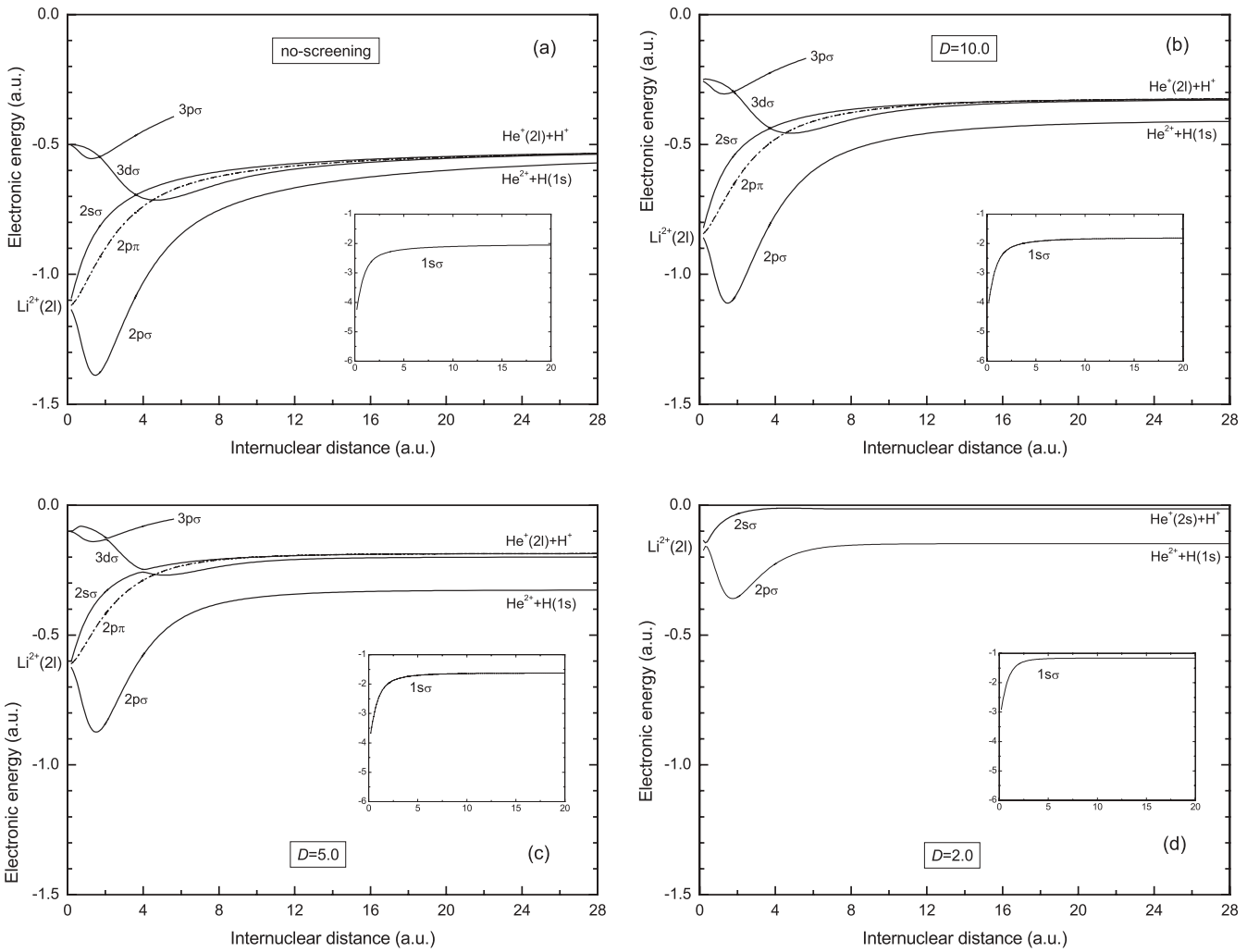


FIG. 1. Electronic energy $\epsilon_n(R)$ as a function of internuclear distance $R$ of the most important molecular orbitals in $(HeH)^{2+}$ collision system. (a) no-screening; (b) $D = 10.0$; (c) $D = 5.0$; (d) $D = 2.0$.

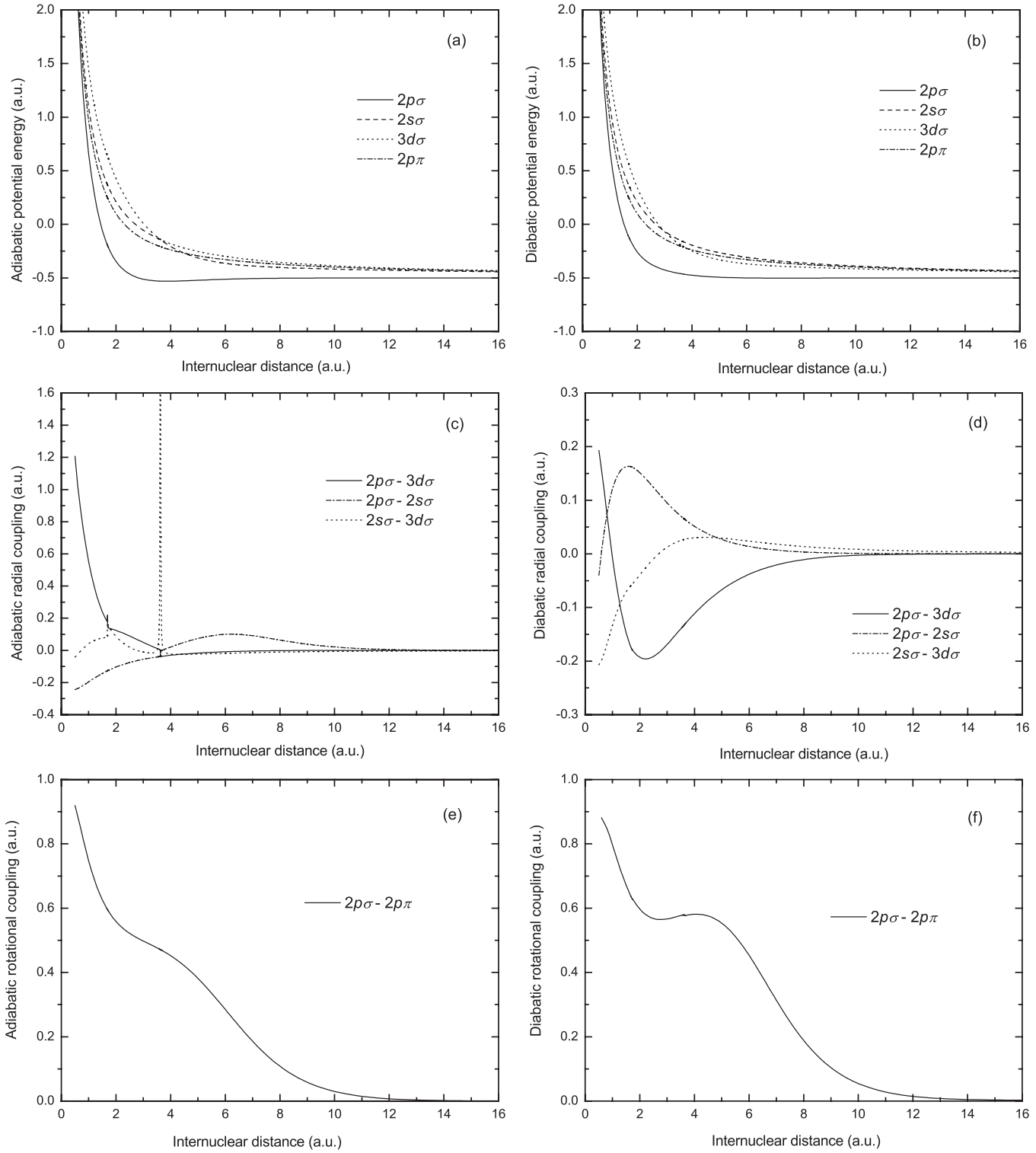


FIG. 2. Potential energies, ETF-corrected radial and rotational couplings (adiabatic and diabatic) as a function of internuclear distance for no-screening case.

the Coulombic potential is screened [40]. A similar avoided crossing is not shown in Figs. 1(b) and 1(c) where $D = 10.0$ and 5.0 because the screening is still weak and the avoided crossing is too close to $R = 0$. Nonetheless, the avoided crossing has very little contribution to the electron-capture cross section in the low-collision-energy region (<5 keV).

In Fig. 2, the adiabatic and diabatic potential energies and the ETF-corrected radial and rotational couplings are presented for the no-screening case. It should be noted that in the adiabatic radial couplings [Fig. 2(c)], in addition to the major peak around $R = 3.6$, which is consistent with the position of the avoided crossing between the $2s\sigma$ and $3d\sigma$ molecular

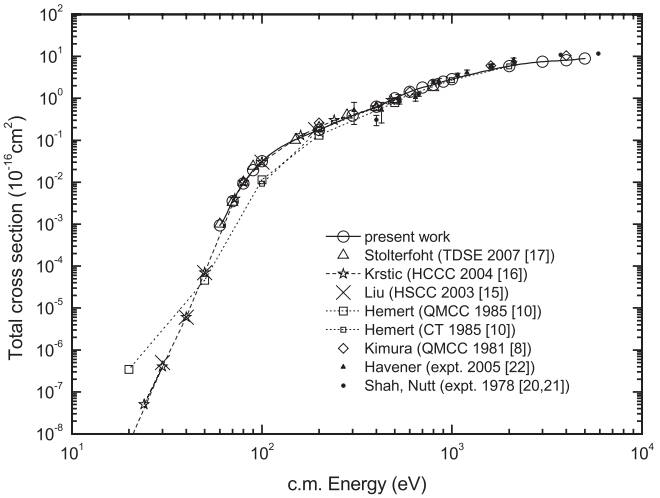


FIG. 3. Total charge-transfer cross sections in $He^{2+} + H(1s) \rightarrow He^{+}(2l) + H^{+}$ collisions for no-screening case. Lines in the figure are for guide of eyes.

orbitals, there is another weak peak around $R = 1.7$, which correlates with the avoided crossing between $3d\sigma$ and $3p\sigma$, as shown in Fig. 1(a).

Using the obtained diabatic potentials and coupling matrix elements with the MRD-CI approach, the QMOCC method, described in Sec. II A, is applied to calculate the charge-transfer cross sections for $He^{2+} + H(1s) \rightarrow He^{+}(2l) + H^{+}$ collisions in the center-of-mass collision-energy region from 60 eV to 5 keV, and the total cross sections for the no-screening case in comparison with existing data, both theoretical and experimental, are presented in Fig. 3. In the calculated energy region, our results are in very good agreement with other theoretical works except with those from Hemert [10] below 200 eV. This discrepancy in the lower-energy region might be attributed to both the difference in the treatment of the electron translation (Vaaben and Taulbjerg type ETF used in Hemert's approach [10]) and the computational accuracy in the calculation of the potential energy surfaces in early years. In comparison, as pointed out by Krstic [16], the hyperspherical coupled-channel method applied by Liu *et al.* [15] is not only a numerically intensive approach to the

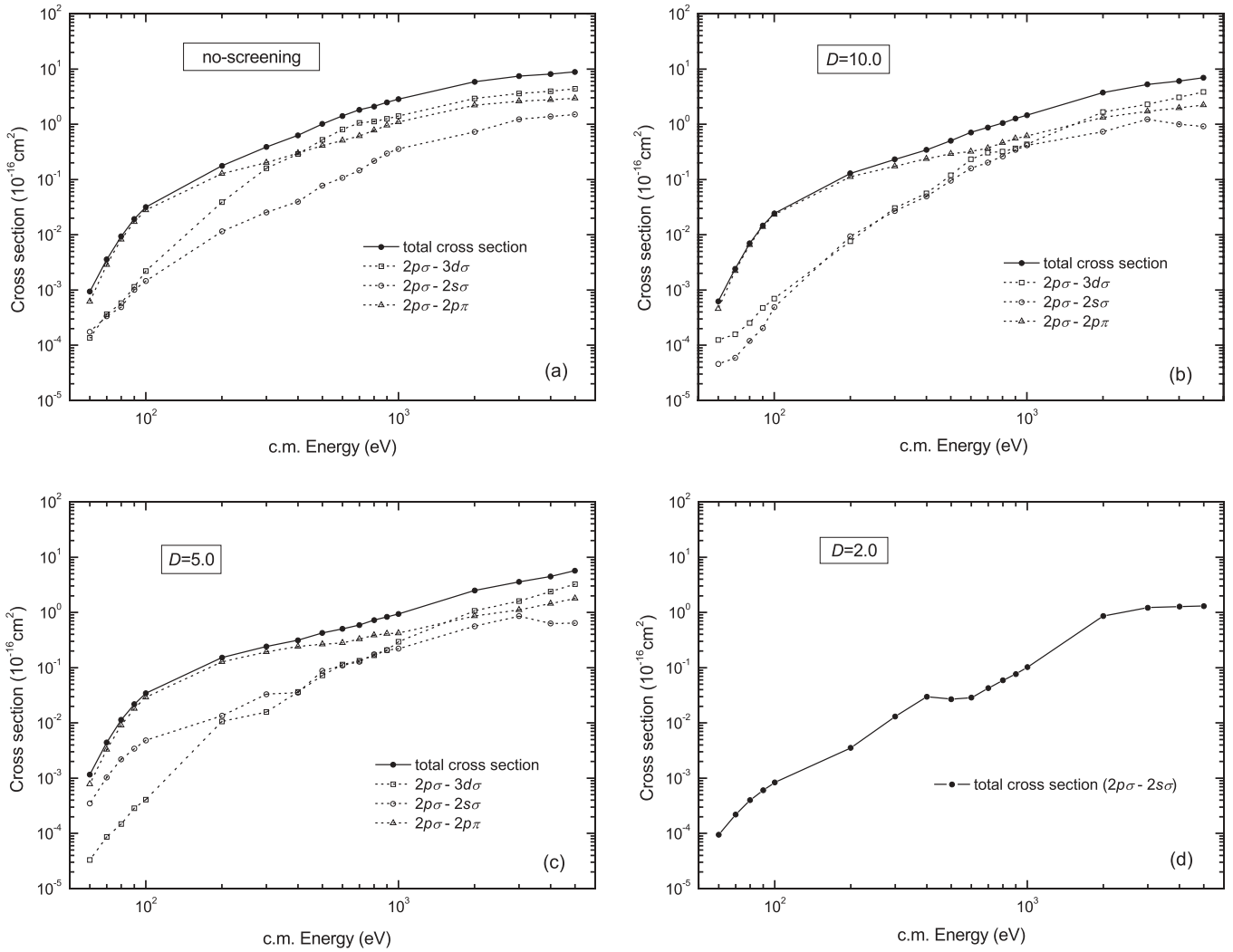


FIG. 4. Total and state-selective charge-transfer cross sections in $He^{2+} + H(1s) \rightarrow He^{+}(2l) + H^{+}$ collisions for no-screening case and screened Coulomb potentials with $D = 10.0, 5.0, 2.0$.

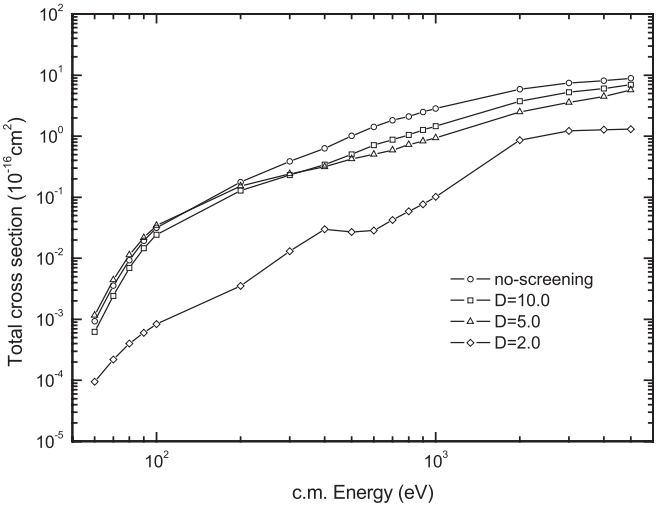


FIG. 5. Total charge-transfer cross sections in $He^{2+} + H(1s) \rightarrow He^{+}(2l) + H^{+}$ collisions for no-screening case and Debye length $D = 10.0, 5.0, 2.0$.

dynamics of three-body systems, but also can, similarly to the hidden-crossings coupled-channel approach, establish the correct boundary conditions as $R \rightarrow \infty$ without using ETF's; therefore, higher accuracy over standard MOCC methods should be achieved.

The total and state-selective cross sections for the screened cases with Debye length $D = 10.0,5.0,2.0$ are calculated similarly and presented in Figs. 4(a)–4(d). In Fig. 5, we compare the total cross sections for both unscreened and screened cases. For the unscreened case, as shown in Fig. 4(a), we found that the radial coupling between $2p\sigma$ and $3d\sigma$ is of the most importance at collision energies 600 eV and above. Although in this energy region the contribution of rotational coupling between $2p\sigma$ and $2p\pi$ is also comparable, an extended calculation to 10 keV (not presented in this work) has shown that the coupling $2p\sigma$ to $3d\sigma$ is dominant at higher energy. However, the contribution of the coupling $2p\sigma$ to $3d\sigma$ decreases exponentially as the impact energy decreases, while that of $2p\sigma$ to $2p\pi$ gains importance gradually and becomes dominant from 60 to 200 eV. Similar behavior has also been observed in the screened cases with $D = 10.0$ and 5.0, except that the upper limit of the dominant region of $2p\sigma$ to $2p\pi$ extends to 500 and 800 eV, respectively.

In Fig. 5, we notice that at collision energies around 1 keV the total cross section decreases as the Debye length $D$

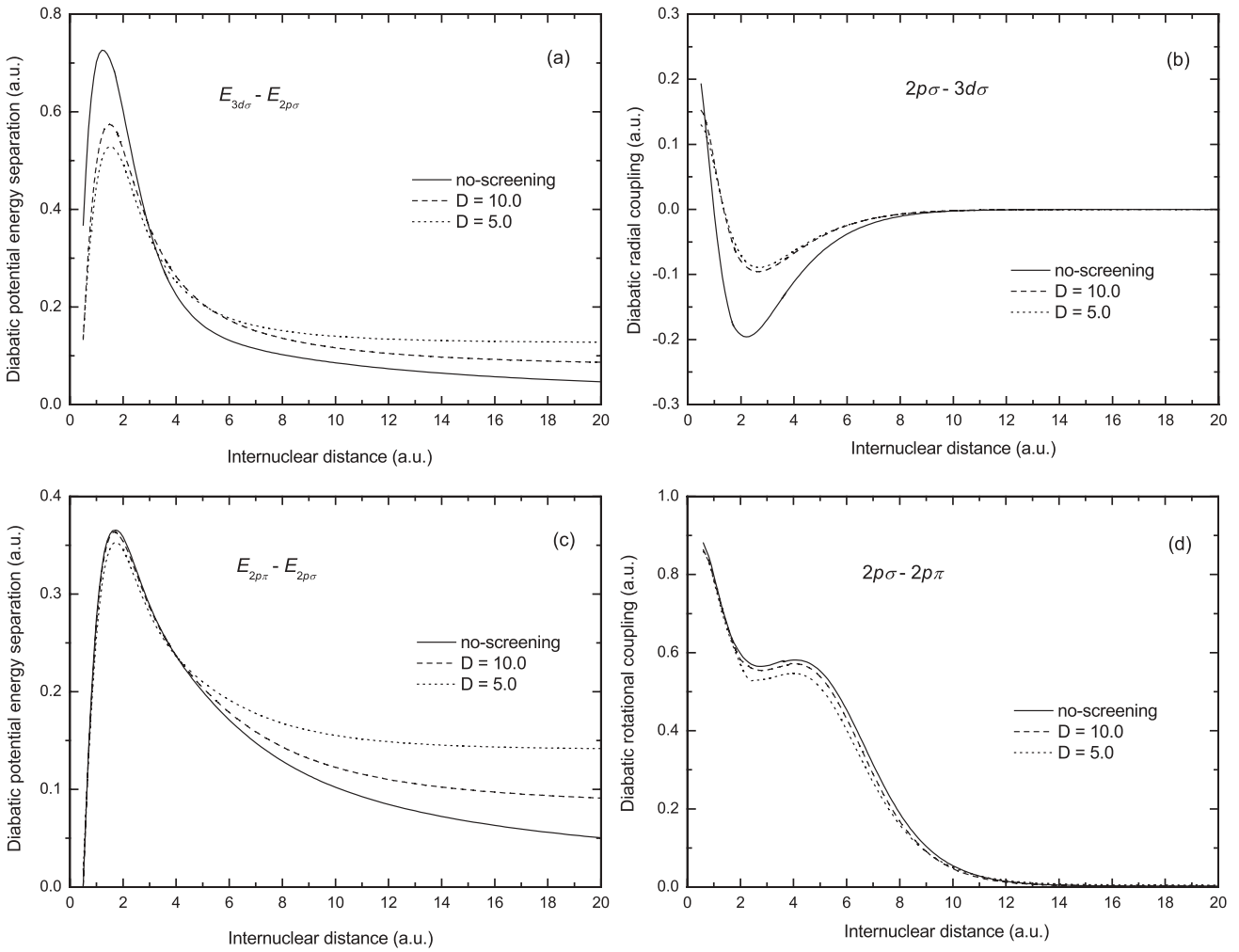


FIG. 6. Diabatic potential energy separations and coupling matrix elements between $2p\sigma$ and $3d\sigma$, $2p\sigma$ and $2p\pi$ with different screening parameters.

decreases, especially for $D = 2.0$, where the total cross section is much smaller than the others since $2p\sigma$-$2s\sigma$ is the only channel permitted with such strong screening. Similar behavior has also been observed in a much higher-energy region (10–300 keV) in Liu *et al.*'s work [23]. However, the total cross sections have no such obvious order at collision energies around 100 eV and below. For example, at 80 eV the total cross section with $D = 5.0$ is larger than that for the no-screening case and for $D = 10.0$. The behavior of the total cross sections with various screening parameters can be qualitatively understood by comparing the diabatic potential energy separations and the coupling matrix elements, as presented in Fig. 6. Two major contributions to the total cross section at collision energies around 1 keV, the radial coupling $2p\sigma$-$3d\sigma$ and the rotational coupling $2p\sigma$-$2p\pi$, both have decreasing matrix elements in the most important internuclear region when $D$ decreases, as shown in Figs. 6(b) and 6(d). Therefore, the behavior of the total cross sections at higher collision energies could be expected because in this energy region the coupling matrix elements are the determinant factors and the potential energy separations are much less important. At lower collision energies around 100 eV and below, things are complicated because both the coupling matrix elements and the potential energy separations become important. Although the rotational coupling $2p\sigma$-$2p\pi$, which dominates in this energy region, has decreasing matrix elements when $D$ decreases, the corresponding potential energy separation increases at large internuclear distance and decreases at small internuclear distance, as shown in Fig. 6(c). The competition between the coupling matrix elements and potential energy separations makes the order of the total cross sections difficult to predict at the lower collision energies.

### B. $He^{2+} + H(1s) \rightarrow He^{+}(1s) + H^{+} + h\nu$ collisions

As the cross sections continue to drop rapidly at lower energies (roughly below 40 eV, i.e., Krstic [16] and Liu *et al.*'s work [15] in Fig. 3), the radiative charge transfer $He^{2+} + H(1s) \rightarrow He^{+}(1s) + H^{+} + h\nu$ will become dominant. The two molecular orbitals involved in this process are the $2p\sigma$ and $1s\sigma$ states. The electronic energy separations and dipole matrix elements are illustrated in Figs. 7 and 8, respectively. In Fig. 9, the calculated transition probability $A(R)$ is presented. Using the optical-potential method and the semiclassical method described in Sec. II B, we obtained the charge-transfer cross sections in the energy range from $10^{-4}$ to 1 eV and 1 to $10^{2}$ eV, respectively, as shown in Fig. 10. The cross sections for the no-screening case (solid line in Fig. 10) are in good agreement with the results of West *et al.* [9]. Rich resonance structures evident at energies below about 0.4 eV are observed for all the unscreened and screened cases; they are due to the transient vibrational and rotational states in the entrance channel $2p\sigma$. The calculated cross sections demonstrate a decreasing trend in the studied energy region from $10^{-4}$ to $10^{2}$ eV as the Debye length $D$ decreases. This is mainly because the electronic energy separation between the $2p\sigma$ and $1s\sigma$ states is reduced (Fig. 7), thus causing a reduction of the transition probability $A(R)$ [Eq. (8)], as shown in Fig. 9. The decrements of the dipole matrix elements (Fig. 8) at $R > 3.0$ when $D$ decreases also enhance this trend.

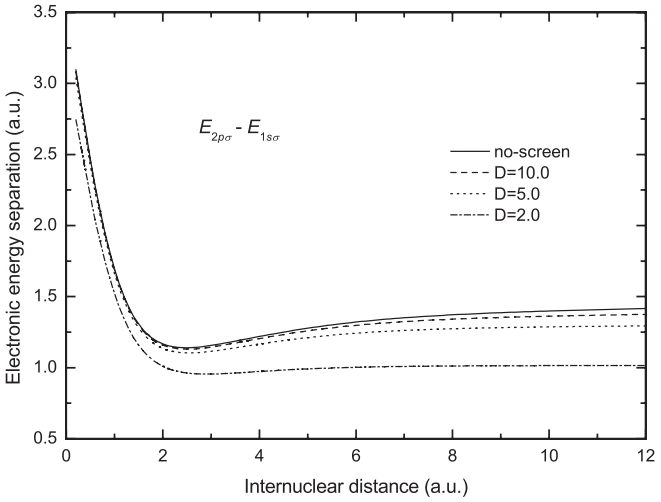


FIG. 7. Electronic energy separation between the $2p\sigma$ and $1s\sigma$ states of $(HeH)^{2+}$.

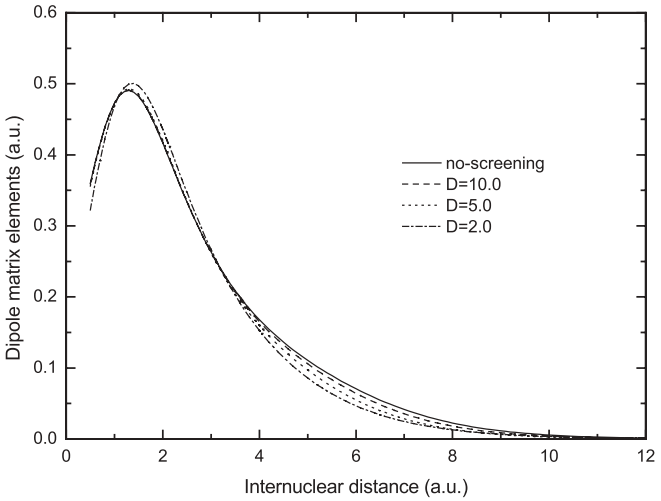


FIG. 8. Dipole matrix elements between the $2p\sigma$ and $1s\sigma$ states of $(HeH)^{2+}$.

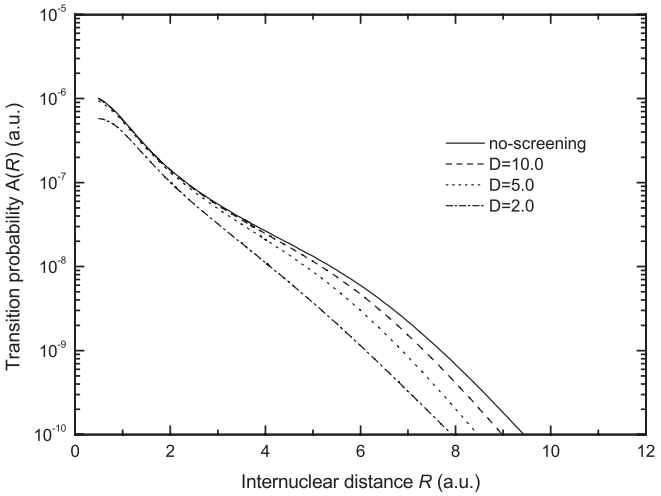


FIG. 9. Transition probability A($R$) between the $2p\sigma$ and $1s\sigma$ states of $(HeH)^{2+}$.

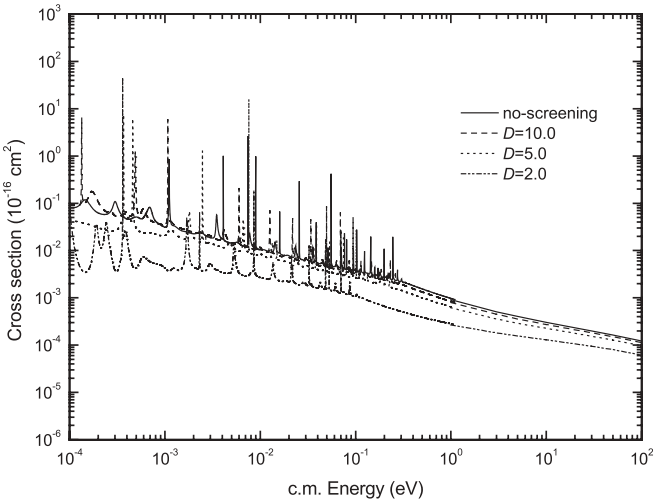


FIG. 10. Radiative charge-transfer cross sections in $He^{2+} + H(1s) \rightarrow He^{+}(1s) + H^{+} + h\nu$ collisions for $D = 10.0$, 5.0, 2.0 and no-screening case. The cross sections are obtained by employing the optical-potential method ($10^{-4}$ to 1 eV) and the semiclassical method (1 to $10^{2}$ eV).

## IV. SUMMARY

The goal of the present work has been to provide accurate knowledge of the effects of Coulomb interaction screening on the total and state-selective cross sections for charge transfer in $He^{2+} + H(1s)$ collisions in the low-energy region. Toward this end we assume that the $(HeH)^{2+}$ collision system is embedded in a Debye plasma and the screened Coulomb interaction is described by the Debye-Hückel potential. The *ab initio* adiabatic potential and coupling matrix elements are obtained by using the MRD-CI package. The QMOCC approach has been applied to calculate the total and state-selective cross sections in the nonradiative charge-transfer process (1) from 60 eV to 5 keV. For the radiative charge-transfer process (2), the optical-potential method and the semiclassical method have been applied in the collision energy range from $10^{-4}$ to 1 eV and 1 to $10^{2}$ eV, respectively. In both processes, the total cross sections generally demonstrate a decreasing trend as the Debye length $D$ decreases, except that there is no such clear trend at energies about 100 eV and below in the nonradiative charge transfer process (1). The behavior of the cross sections can be attributed to the introduced changes of the potential energy separations and coupling matrix elements with different screening parameters.

## ACKNOWLEDGMENTS

This work was partly supported by the National Science Foundation of China (Grants No. 10875017, No. 10974021, No. 10979007, No. 10734140, and No. 2005CB724500).

[1] J. C. Weisheit, in *Applied Atomic Collision Physics*, edited by C. F. Barnett and M. F. A. Harrison (Academic, New York, 1984), Vol. 2.
[2] E. L. Pollock and J. C. Weisheit, in *Spectral Line Shapes*, edited by F. Rostas (Walter de Gruyter, New York, 1985), Vol. 3, p. 181.
[3] J. C. Weisheit, Adv. At. Mol. Phys. **25**, 101 (1988).
[4] M. S. Murillo and J. C. Weisheit, in *Strongly Coupled Plasma Physics*, edited by H. M. Van Horn (University of Rochester Press, Rochester, NY, 1993), p. 233.
[5] M. S. Murillo, in *Atomic Processes in Plasmas*, edited by A. L. Osterheld and W. H. Goldstein, AIP Conf. Proc. No. 381 (AIP, New York, 1996), p. 231.
[6] M. S. Murillo and J. C. Weisheit, Phys. Rep. **302**, 1 (1998).
[7] R. K. Janev, *Atomic and Molecular Processes in Fusion Edge Plasmas* (Plenum, New York, 1995).
[8] M. Kimura and W. R. Thorson, Phys. Rev. A **24**, 3019 (1981).
[9] B. W. West, Neal F. Lane, and James S. Cohen, Phys. Rev. A **26**, 3164 (1982).
[10] M. C. van Hemert, E. F. van Dishoeck, J. A. van der Hart, and F. Koike, Phys. Rev. A **31**, 2227 (1985).
[11] T. G. Winter, Phys. Rev. A **37**, 4656 (1988).
[12] H. Fukuda and T. Ishihara, Phys. Rev. A **46**, 5531 (1992).
[13] L. F. Errea, C. Harel, H. Jouin, J. M. Maidagan, L. Mendez, B. Pons, and A. Riera, Phys. Rev. A **46**, 5617 (1992).
[14] R. K. Janev, J. Pop-Jordanov, and E. A. Solov'ev, J. Phys. B **30**, L353 (1997).
[15] C. N. Liu, A. T. Le, T. Morishita, B. D. Esry, and C. D. Lin, Phys. Rev. A **67**, 052705 (2003).
[16] P. S. Krstic, J. Phys. B **37**, L217 (2004).
[17] N. Stolterfoht, R. Cabrera-Trujillo, Y. Ohrn, E. Deumens, R. Hoekstra, and J. R. Sabin, Phys. Rev. Lett. **99**, 103201 (2007).
[18] T. Minami, T.-G. Lee, M. S. Pindzola, and D. R. Schultz, J. Phys. B **41**, 135201 (2008).
[19] W. L. Fite, A. C. H. Smith, and R. F. Stebbings, Proc. R. Soc. London, Ser. A **268**, 527 (1962)
[20] M. B. Shah and H. B. Gilbody, J. Phys. B **11**, 121 (1978).
[21] W. L. Nutt, R. W. McCullough, K. Brady, M. B. Shah, and H. B. Gilbody, J. Phys. B **11**, 1457 (1978).
[22] C. C. Havener, R. Rejoub, and P. S. Krstic, Phys. Rev. A **71**, 042707 (2005).
[23] L. Liu, J. G. Wang, and R. K. Janev, Phys. Rev. A **77**, 032709 (2008).
[24] R. J. Buenker and S. D. Peyerimhoff, Theor. Chim. Acta **35**, 33 (1974); **39**, 217 (1975); R. J. Buenker, Int. J. Quantum Chem. **29**, 435 (1986); S. Krebs and R. J. Buenker, J. Chem. Phys. **103**, 5613 (1995).
[25] Y. Wu, J. G. Wang, P. S. Krstic, and R. K. Janev, J. Phys. B **43**, 201003 (2010).
[26] M. Kimura and N. F. Lane, Adv. At. Mol. Opt. Phys. **26**, 79 (1990).
[27] B. Zygelman, D. L. Cooper, M. J. Ford, A. Dalgarno, J. Gerratt, and M. Raimondi, Phys. Rev. A **46**, 3846 (1992).
[28] J. G. Wang, P. C. Stancil, A. R. Turner, and D. L. Cooper, Phys. Rev. A **67**, 012710 (2003); **69**, 062702 (2004).
[29] B. R. Johnson, J. Comput. Phys. **13**, 445 (1973).
[30] T. G. Heil, S. E. Butler, and A. Dalgarno, Phys. Rev. A **27**, 2365 (1983).
[31] D. L. Cooper, N. J. Clarke, P. C. Stancil, and B. Zygelman, Adv. Quantum Chem. **40**, 37 (2001).

[32] B. H. Brandsen and M. R. C. McDowell, *Charge Exchange and the Theory of Ion-Atom Collision* (Clarendon Press, Oxford, 1992).
[33] A. R. Turner, D. L. Cooper, J. G. Wang, and P. C. Stancil, Phys. Rev. A **68**, 012704 (2003).
[34] L. F. Errea, L. Mendez, and A. Riera, J. Phys. B **15**, 101 (1982).
[35] M. C. Bacchus-Montabonel and P. Ceyzeriat, Phys. Rev. A **58**, 1162 (1998).
[36] B. Zygelman and A. Dalgarno, Phys. Rev. A **38**, 1877 (1988).
[37] D. R. Bates, Mon. Not. R. Astron. Soc. **111**, 303 (1951).
[38] P. C. Stancil and B. Zygelman, Astrophys. J. **472**, 102 (1996).
[39] L. B. Zhao, J. G. Wang, P. C. Stancil, J. P. Gu, H.-P. Liebermann, R. J. Buenker, and M. Kimura, J. Phys. B **39**, 5151 (2006).
[40] F. J. Rogers, H. C. Graboske, Jr., and D. J. Harwood, Phys. Rev. A **1**, 1577 (1970).